Article

Metallacryptate Single-Molecule Magnets: Effect of Lower Molecular Symmetry on Blocking Temperature

Curtis M. Zaleski, Ezra C. Depperman, Catherine Dendrinou-Samara, Maria Alexiou, Jeff W. Kampf, Dimitris P. Kessissoglou, Martin L. Kirk, and Vincent L. Pecoraro

J. Am. Chem. Soc., **2005**, 127 (37), 12862-12872• DOI: 10.1021/ja050951i • Publication Date (Web): 26 August 2005

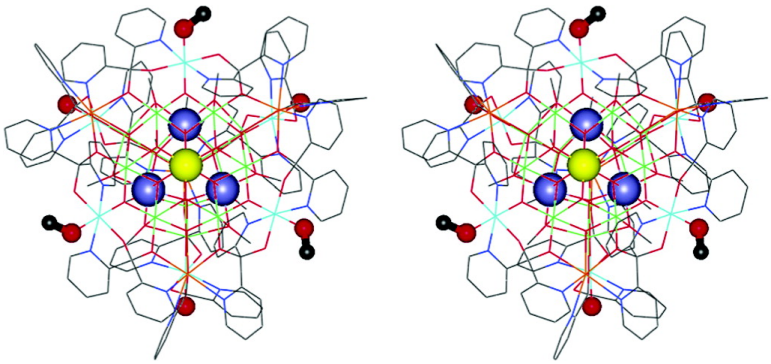

J|A|C|S
ARTICLES
Published on Web 08/26/2005

Metallacryptate Single-Molecule Magnets: Effect of Lower Molecular Symmetry on Blocking Temperature

Curtis M. Zaleski,[§] Ezra C. Depperman,[†] Catherine Dendrinou-Samara,[‡] Maria Alexiou,[‡] Jeff W. Kampf,[§] Dimitris P. Kessissoglou,*[,‡] Martin L. Kirk,*[,†] and Vincent L. Pecoraro*[,§]

Contribution from the Department of Chemistry, University of Michigan, Ann Arbor, Michigan 48109-1055, Department of Chemistry, The University of New Mexico, Albuquerque, New Mexico 87131-0001, and Department of General and Inorganic Chemistry, Aristotle University of Thessaloniki, Thessaloniki 54124, Greece

Received February 14, 2005; E-mail: kessisog@chem.auth.gr; mkirk@unm.edu; vlpec@umich.edu

Abstract: The structural characterization of complexes $[Mn^{II}_4Mn^{III}_{22}(pdol)_{12}(OCH_3)_{12}(O)_{16}(N_3)_6]$ (**1**) and $[Mn^{II}_4Mn^{III}_{22}(pdol)_{12}(OCH_3)_{12}(O)_{16}(OH)_2(H_2O)(OCH_3)_3]\cdot ClO_4\cdot 5CH_3OH$ (**2**), where $pdol^{2-}$ is di-2-pyridyl methanediol, reveals that each has a metallacryptand shell that encapsulates a manganese oxide core. Variable-temperature direct current magnetic susceptibility measurements on **2** indicate a paramagnetic ground state that results from an overall antiferromagnetic interaction in the cluster, with χT values decreasing from 300 K (51.2 cm^3 K mol^{-1}) to 2 K (19.8 cm^3 K mol^{-1}). Variable-temperature alternating current magnetic susceptibility measurements imply that both **1** and **2** behave as single-molecule magnets. Fitting the frequency-dependent out-of-phase magnetic susceptibility to the Arrhenius equation yields an effective energy barrier, U_{eff}, to magnetization relaxation of 16.5 ± 0.7 K (11.5 ± 0.5 cm^{-1}) for **1** and 36.2 ± 2.0 K (25.1 ± 1.4 cm^{-1}) for **2**. The larger value for **2** is in agreement with the lower molecular symmetry, larger magnetoanisotropy, and higher ground spin state of **2** compared to those of **1**. This observation suggests a new strategy for increasing the blocking temperatures in high-nuclearity manganese clusters.

Introduction

The intense study of metallamacrocycles over the past two decades has been catalyzed by the fact that this class of molecular materials is relevant to a variety of modern chemical interests, including catalysis,[1,2] sensors,[3−6] molecular recognition,[7,8] and chiral building blocks for one-, two-, and three-dimensional solids.[9−11] Examples of metallamacrocycles include metallacrowns,[12−15] molecular squares,[16,17] metallahelicates,[18,19] metallacryptates and metallacryptands,[20−24] and metallacalixarenes.[25,26] Metallacrowns (MC) were first described in 1989 by Lah and Pecoraro[12,13] and are among the earliest described metallamacrocycles. The original metallacrown structures described contain a $-[M-N-O]_n-$ repeat unit, where $n = 3$, 4, and 5.[15] The nomenclature for metallacrowns is derived from that of crown ethers, where the methylene carbons are replaced by a metal ion and a heteroatom, typically nitrogen. While the earliest metallacrowns focused on 9-MC-3 ($n = 3$),[12] 12-MC-4 ($n = 4$),[13,27] and 15-MC-5 ($n = 5$)[14,28,29] structure types, these

§ University of Michigan.
† The Universityof New Mexico.
‡ Aristotle University of Thessaloniki.

(1) Fujita, M.; Kwon, Y. J.; Washizu, S.; Ogura, K. *J. Am. Chem. Soc.* **1994**, *116*, 1151.
(2) Merlau, M. L.; del Pilar Mejia, M.; Nguyen, S. T.; Hupp, J. T. *Angew. Chem., Int. Ed.* **2001**, *40*, 4239.
(3) Piotrowski, H.; Polborn, K.; Hilt, G.; Severin, K. *J. Am. Chem. Soc.* **2001**, *123*, 2699.
(4) Piotrowski, H.; Severin, K. *Proc. Natl. Acad. Sci.* **2002**, *99*, 4997.
(5) Grote, Z.; Lehaire, M.-L.; Scopelliti, R.; Severin, K. *J. Am. Chem. Soc.* **2003**, *125*, 13638.
(6) Chang, S. H.; Chung, K.-B.; Slone, R. V.; Hupp, J. T. *Synth. Met.* **2001**, *117*, 215.
(7) Chen, H.; Maestre, M. F.; Fish, R. H. *J. Am. Chem. Soc.* **1995**, *117*, 3631.
(8) Chen, H.; Ogo, S.; Fish, R. H. *J. Am. Chem. Soc.* **1996**, *118*, 4993.
(9) Cutland-Van Noord, A. C.; Kampf, J. W.; Pecoraro, V. L. *Angew. Chem., Int. Ed.* **2002**, *41*, 4668.
(10) Bodwin, J. J.; Pecoraro, V. L. *Inorg. Chem.* **2000**, *39*, 3434.
(11) Moon, M.; Kim, I.; Lah, M. S. *Inorg. Chem.* **2000**, *39*, 2710.
(12) Pecoraro, V. L. *Inorg. Chim. Acta* **1989**, *155*, 171.
(13) Lah, M. S.; Pecoraro, V. L. *J. Am. Chem. Soc.* **1989**, *111*, 7258.
(14) Kessissoglou, D. P.; Kampf, J. W.; Pecoraro, V. L. *Polyhedron* **1994**, *13*, 1379.
(15) Pecoraro, V. L.; Stemmler, A. J.; Gibney, B. R.; Bodwin, J. J.; Wang, H.; Kampf, J. W.; Barwinski, A. In *Progress in Inorganic Chemistry*; Karlin, K. D., Ed.; John Wiley & Sons: New York, 1997; Vol. 45, p 83.
(16) Fujita, M.; Yazaki, J.; Ogura, K. *J. Am. Chem. Soc.* **1990**, *112*, 5645.
(17) Fujita, M. *Chem. Soc. Rev.* **1998**, *27*, 417.
(18) Johnson, J. A.; Kampf, J. W.; Pecoraro, V. L. *Angew. Chem., Int. Ed.* **2003**, *42*, 546.
(19) Matthews, C. J.; Onions, S. T.; Morata, G.; Davis, L. J.; Heath, S. L.; Price, D. J. *Angew. Chem., Int. Ed.* **2003**, *42*, 3166.
(20) Saalfrank, R. W.; Dresel, A.; Seitz, V.; Trummer, S.; Hampel, F.; Teichert, M.; Stalke, D.; Stadler, C.; Daub, J.; Schunemann, V.; Trautwein, A. X. *Chem. Eur. J.* **1997**, *3*, 2058.
(21) Saalfrank, R. W.; Seitz, V.; Caulder, D. L.; Raymond, K. N.; Teichert, M.; Stalke, D. *Eur. J. Inorg. Chem.* **1998**, 1313.
(22) Catalano, V. J.; Malwitz, M. A. *Inorg. Chem.* **2002**, *41*, 6553.
(23) Dendrinou-Samara, C.; Alexiou, M.; Zaleski, C. M.; Kampf, J. W.; Kirk, M. L.; Kessissoglou, D. P.; Pecoraro, V. L. *Angew. Chem., Int. Ed.* **2003**, *42*, 3763.
(24) Beer, P. D.; Cheetham, A. G.; Drew, M. G. B.; Fox, O. D.; Hayes, E. J.; Rolls, T. D. *Dalton Trans.* **2003**, *2003*, 603.
(25) Rauter, H.; Hillgeris, E. C.; Erxleben, A.; Lippert, B. *J. Am. Chem. Soc.* **1994**, *116*, 616.
(26) Rauterkus, M. J.; Krebs, B. *Angew. Chem., Int. Ed.* **2004**, *43*, 1300.
(27) Halfen, J. A.; Bodwin, J. J.; Pecoraro, V. L. *Inorg. Chem.* **1998**, *37*, 5416.
(28) Stemmler, A. J.; Kampf, J. W.; Pecoraro, V. L. *Angew. Chem., Int. Ed. Engl.* **1996**, *35*, 2841.
(29) Stemmler, A. J.; Barwinski, A.; Baldwin, M. J.; Young, V.; Pecoraro, V. L. *J. Am. Chem. Soc.* **1996**, *118*, 11962.

10.1021/ja050951i CCC: $30.25

metallamacrocycles are now quite diverse and include expanded metallacrowns,[3] metallacoronates,[30] azametallacrowns,[31] and expanded azametallacrowns.[32] In these structures, carbon atoms are included in the repeat unit (expanded metallacrowns), both of the heteroatoms are oxygen with carbon atom extenders (metallacoronates), or the oxygen atom has been replaced by a nitrogen atom to give a −[M−N−N]− repeat unit (azametallacrowns and expanded azametallacrowns). Organometallic derivatives have broadened the structural diversity of this class of molecules even further. Now metallacrowns with varying ring sizes are known, including 12-MC-3,[3,32] 12-MC-6,[33−35] 15-MC-6,[30] 16-MC-4,[36] 16-MC-8,[33] 18-MC-6,[31,37] 22-MC-8,[38] 24-MC-6,[39,40] 24-MC-8,[41−43] 30-MC-10,[44] and 36-MC-12.[45]

One advantage of the metallacrown structure topology is that many metal centers are placed in close proximity, and they can be exploited for a variety of applications. Metallacrowns have been studied for their anion binding,[46−48], molecular recognition,[7,8] ability to stabilize highly active molecules,[49,50] as sensors,[3,4] as antibacterial compounds,[51,52] and as building blocks for extended solids.[9−11] Furthermore, metallacrowns and related structures are now being intensely studied for their unusual magnetic properties. Initially, studies were directed toward providing a basic understanding of the gross magnetic exchange interactions[53] in these cluster compounds. However, metallacrowns are now recognized to be a new entry into the class of molecules known as single-molecule magnets (SMMs).[23]

Single-molecule magnets are a relatively new class of molecules and represent an exciting new area of fundamental research.[54] With properties that merge the classical and quantum regimes, potential applications range from high-density storage devices to quantum computers.[54] Gatteschi, Hendrickson, Christou, and co-workers characterized $[Mn_{12}O_{12}(O_2CCH_3)_{16}(H_2O)_4]\cdot CH_3CO_2H\cdot 3H_2O$ {Mn_{12}OAc} as the first single-molecule magnet in 1993.[55,56] Single-molecule magnet behavior in metallic clusters is derived from a large spin ground state and a large negative axial magnetoanisotropy, which is expressed as the molecular zero-field splitting parameter, D. A large spin ground state (S) and negative magnetoanisotropy conspire to create an energy barrier to magnetization relaxation, represented by the blocking temperature, T_B, which is proportional to the square of the ground-state spin and directly proportional to the zero-field splitting in the ground state ($E = S^2|D|$). Below this blocking temperature, the relaxation process slows sufficiently that each molecule behaves as a single magnetic domain (i.e., a superparamagnet) and the barrier to magnetization relaxation can be probed by alternating current (ac) magnetic susceptibility experiments and the construction of hysteresis loops in the direct current (dc) magnetization.[56] Manganese clusters possessing a large percentage of Mn^{III} ions have been shown to represent ideal clusters for study, as the number of unpaired spins per ion is high ($S = 2$) and Mn^{III} is known to possess a large single-ion anisotropy, with $D < 0$.[57]

Much of the work on SMMs has focused on the original Mn_{12}-OAc cluster, and many of the subsequent studies have concentrated on Mn_4 and Mn_{12} clusters possessing carboxylate ligands.[54,58] Recently there has been a surge in the number of characterized SMMs with manganese cluster sizes greater than 12, though most of these clusters are either entirely, or at least partially, carboxylate based. Cluster sizes have been reported with Mn_{16},[59−61] Mn_{18},[62,63] Mn_{21},[63,64] Mn_{22},[65] Mn_{25},[66] Mn_{26},[23,67,68] Mn_{30},[69,70] and Mn_{84}.[71] There are few examples of large manganese clusters that contain no carboxylate ligands.[23,66−68] Smaller manganese clusters have also been reported in the Mn_4−Mn_{12} range, such as Mn_5,[72] Mn_6,[61,73] Mn_7,[74] Mn_8,[75−77] and

(30) Saalfrank, R. W.; Low, N.; Hampel, F.; Stachel, H. *Angew. Chem., Int. Ed. Engl.* **1996**, *35*, 2209.
(31) Kwak, B.; Rhee, H.; Park, S.; Lah, M. S. *Inorg. Chem.* **1998**, *37*, 3599.
(32) Smith, D. P.; Baralt, E.; Morales, B.; Olmstead, M. M.; Maestre, M. F.; Fish, R. H. *J. Am. Chem. Soc.* **1992**, *114*, 10647.
(33) Saalfrank, R. W.; Bernt, I.; Uller, E.; Hampel, F. *Angew. Chem., Int. Ed. Engl.* **1997**, *36*, 2482.
(34) Mandal, S. K.; Young, V.; Que, L. *Inorg. Chem.* **2000**, *39*, 1831.
(35) Saalfrank, R. W.; Bernt, I.; Chowdhry, M. M.; Hampel, F.; Vaughan, G. B. M. *Chem. Eur. J.* **2001**, *7*, 2765.
(36) Sheldrick, W. S.; Hagen-Eckhard, H. S.; Heeb, S. *Inorg. Chim. Acta* **1993**, *206*, 15.
(37) El Fallah, M. S.; Rentschler, E.; Caneschi, A.; Sessoli, R.; Gatteschi, D. *Inorg. Chem.* **1996**, *35*, 3723.
(38) Saalfrank, R. W.; Maid, H.; Mooren, N.; Hampel, F. *Angew. Chem., Int. Ed.* **2002**, *41*, 304.
(39) Blake, A. J.; Gould, R. O.; Milne, P. E. Y.; Winpenny, R. E. P. *J. Chem. Soc., Chem. Commun.* **1991**, 1453.
(40) Yamanari, K.; Yamamoto, S.; Ito, R.; Kushi, Y.; Fuyuhiro, A.; Kubota, N.; Fukuo, T.; Arakawa, R. *Angew. Chem., Int. Ed.* **2001**, *40*, 2268.
(41) Saarinen, H.; Orama, M. *Acta Chem. Scand.* **1998**, *52*, 1209.
(42) Dendrinou-Samara, C.; Zaleski, C. M.; Evagorou, A.; Kampf, J. W.; Pecoraro, V. L.; Kessissoglou, D. P. *Chem. Commun.* **2003**, 2668.
(43) Lin, S.; Liu, S.-X.; Chen, Z.; Lin, B.-Z.; Gao, S. *Inorg. Chem.* **2004**, *43*, 2222.
(44) Liu, S.; Lin, S.; Lin, B.; Lin, C.; Huang, J. *Angew. Chem., Int. Ed.* **2001**, *40*, 1084.
(45) John, R. P.; Lee, K.; Lah, M. S. *Chem. Commun.* **2004**, 2660.
(46) Cutland, A. D.; Malkani, R. G.; Kampf, J. W.; Pecoraro, V. L. *Angew. Chem., Int. Ed.* **2000**, *39*, 2689.
(47) Cutland, A. D.; Halfen, J. A.; Kampf, J. W.; Pecoraro, V. L. *J. Am. Chem. Soc.* **2001**, *123*, 6211.
(48) Dendrinou-Samara, C.; Alevizopoulou, L.; Iordanidis, L.; Samaras, E.; Kessissoglou, D. P. *J. Inorg. Biochem.* **2002**, *89*, 89.
(49) Lehaire, M.-L.; Scopelliti, R.; Severin, K. *Inorg. Chem.* **2002**, *41*, 5466.
(50) Lehaire, M.-L.; Scopelliti, R.; Severin, K. *Chem. Commun.* **2002**, 2766.
(51) Alexiou, M.; Tsivikas, I.; Dendrinou-Samara, C.; Pantazaki, A. A.; Trikalitis, P.; Lalioti, N.; Kyriakidis, D. A.; Kessissoglou, D. P. *J. Inorg. Biochem.* **2003**, *93*, 256.
(52) Tsivikas, I.; Alexiou, M.; Pantazaki, A. A.; Dendrinou-Samara, C.; Kyriakidis, D. A.; Kessissoglou, D. P. *Bioinorg. Chem. Appl.* **2003**, *1*, 85.
(53) Stemmler, A. J.; Kampf, J. W.; Kirk, M. L.; Atasi, B. H.; Pecoraro, V. L. *Inorg. Chem.* **1999**, *38*, 2807.
(54) Christou, G.; Gatteschi, D.; Hendrickson, D. N.; Sessoli, R. *MRS Bull.* **2000**, *25*, 66.
(55) Sessoli, R.; Gatteschi, D.; Novak, M. A. *Nature* **1993**, *365*, 141.
(56) Sessoli, R.; Tsai, H.; Schake, A. R.; Wang, S.; Vincent, J. B.; Folting, K.; Gatteschi, D.; Christou, G.; Hendrickson, D. N. *J. Am. Chem. Soc.* **1993**, *115*, 1804.
(57) Bonadies, J. A.; Kirk, M. L.; Lah, M. S.; Kessissoglou, D. P.; Hatfield, W. E.; Pecoraro, V. L. *Inorg. Chem.* **1989**, *28*, 2037.
(58) Gatteschi, D.; Sessoli, R. *Angew. Chem., Int. Ed.* **2003**, *42*, 268.
(59) Price, D. J.; Batten, S. R.; Moubaraki, B.; Murray, K. S. *Chem. Commun.* **2002**, 762.
(60) King, P.; Wernsdorfer, W.; Abboud, K. A.; Christou, G. *Inorg. Chem.* **2004**, *43*, 7315.
(61) Murugesu, M.; Wernsdorfer, W.; Abboud, K. A.; Christou, G. *Angew. Chem., Int. Ed.* **2005**, *44*, 892.
(62) Brechin, E. K.; Boskovic, C.; Wernsdorfer, W.; Yoo, J.; Yamaguchi, A.; Sanudo, E. C.; Concolino, T. E.; Rheingold, A. L.; Ishimoto, H.; Hendrickson, D. N.; Christou, G. *J. Am. Chem. Soc.* **2002**, *124*, 9710.
(63) Sanudo, E. C.; Brechin, E. K.; Boskovic, C.; Wernsdorfer, W.; Yoo, J.; Yamaguchi, A.; Concolino, T. E.; Abboud, K. A.; Rheingold, A. L.; Ishimoto, H.; Hendrickson, D. N.; Christou, G. *Polyhedron* **2003**, *22*, 2267.
(64) Sanudo, E. C.; Wernsdorfer, W.; Abboud, K. A.; Christou, G. *Inorg. Chem.* **2004**, *43*, 4137.
(65) Murugesu, M.; Raftery, J.; Wernsdorfer, W.; Christou, G.; Brechin, E. K. *Inorg. Chem.* **2004**, *43*, 4203.
(66) Murugesu, M.; Habrych, M.; Wernsdorfer, W.; Abboud, K. A.; Christou, G. *J. Am. Chem. Soc.* **2004**, *126*, 4766.
(67) Jones, L. F.; Rechin, E. K.; Collison, D.; Harrison, A.; Teat, S. J.; Wernsdorfer, W. *Chem. Commun.* **2002**, 2974.
(68) Jones, L. F.; Rajaraman, G.; Brockman, J. T.; Murugesu, M.; Sanudo, E. C.; Raftery, J.; Teat, S. J.; Wernsdorfer, W.; Christou, G.; Brechin, E. K.; Collison, D. *Chem. Eur. J.* **2004**, *10*, 5180.
(69) Soler, M.; Rumberger, E.; Folting, K.; Hendrickson, D. N.; Christou, G. *Polyhedron* **2001**, *20*, 1365.
(70) Soler, M.; Wernsdorfer, W.; Folting, K.; Pink, M.; Christou, G. *J. Am. Chem. Soc.* **2004**, *126*, 2156.
(71) Tasiopoulos, A. J.; Vinslava, A.; Wernsdorfer, W.; Abboud, K. A.; Christou, G. *Angew. Chem., Int. Ed.* **2004**, *43*, 2117.
(72) Berlinguette, C. P.; Vaughn, D.; Canada-Vilalta, C.; Galan-Mascaros, J.-R.; Dunbar, K. R. *Angew. Chem., Int. Ed.* **2003**, *42*, 1523.

Mn_9.[75,78,79] In addition, other metal ion clusters have been described as single-molecule magnets, including those that possess vanadium,[80] iron,[81−83] cobalt,[84,85] nickel,[86,87] and very recently binary d/f-block-containing systems with either copper/terbium[88] or manganese/dysprosium.[89,90]

In a previous report,[23] we presented a preliminary characterization of a Mn_{26} metallacryptate (a three-dimensional metallacrown) that exhibits SMM behavior. Herein we provide further magnetic characterization of this $[Mn^{II}_4Mn^{III}_{22}(pdol)_{12}(OCH_3)_{12}(O)_{16}(N_3)_6]$ (**1**) structure while also describing the structural and magnetic characterization of a new metallacryptate structure, $[Mn^{II}_4Mn^{III}_{22}(pdol)_{12}(OCH_3)_{12}(O)_{16}(OH)_2(H_2O)(OCH_3)_3]\cdot ClO_4\cdot 5CH_3OH$ (**2**), where the azide anions are replaced by water, hydroxide, and methoxide. Although all of the Mn ions in **1** and **2** are *chemically* equivalent, the overall symmetry of **2** is lower than that of **1** due to azide anion replacement. In this article, we present a magnetostructural correlation that relates how these ancillary cluster anions and solvent combine to template the structure of the inner tetranuclear cores of **1** and **2**, resulting in the reorientation of core ion Jahn−Teller axes and a related change in core pairwise exchange interactions. This has the interesting effect of altering the ground spin state of the core and concomitantly the cluster, resulting in an enhanced blocking temperature for the less symmetrical **2** compared with **1**. This is a rare example of how changing the identity of the peripheral anions perpetuates significant changes to the magnetic properties without affecting the overall topology of the complex or the oxidation state of the manganese ions.

Experimental Section

Synthesis. *N*,*N*-Dimethylformamide (DMF) was distilled from calcium hydride (CaH_2), and methanol was distilled from magnesium (Mg); both were stored over 3 Å molecular sieves. Dimethyl sulfoxide (DMSO) was used without any further purification. Di-2-pyridyl ketone oxime, di-2-pyridyl ketone, $Mn(ClO_4)_2\cdot 6H_2O$, and $MnCl_2\cdot 4H_2O$ were purchased from Aldrich Chemical Co. and used as received. All chemicals and solvents were reagent grade.

$[Mn^{II}_4Mn^{III}_{22}(pdol)_{12}(\mu_3\text{-}OCH_3)_{12}(\mu_3\text{-}O)_6(\mu_4\text{-}O)_{10}(N_3)_6]$ (1). Procedure 1. Compound **1** was synthesized by adding 10 mmol of the sodium salt of di-2-pyridyl ketone oxime ligand to 15 mmol of $MnCl_2\cdot 4H_2O$ in 40 mL of methanol. A 10 mmol portion of the NaN_3 dissolved in 10 mL of methanol was added. The resulting dark red-brown solution was reduced to 20 mL after 5 h of stirring. After 24 h, black crystals suitable for X-ray diffraction studies were obtained by slow evaporation. These crystals have been structurally characterized with the formula $Mn^{II}_2Mn^{III}_2(pko)_2(pdol)_2(N_3)_6(CH_3OH)_2$ (Hpko = di-2-pyridyl ketone oxime, H_2pdol = di-2-pyridyl methanediol) [manuscript in preparation]. After 4 days, red/black octahedral crystals were deposited from the remaining mother liquid. These crystals have been structurally characterized with the formula $Mn_{26}(O_{16})(pdol)_{12}(N_3)_6(CH_3O)_{12}$. Analytical data: found C, 36.20; H, 3.00; N, 12.10; $C_{144}H_{132}N_{42}O_{52}Mn_{26}$ (fw = 4711.36) requires C, 36.68; H, 2.80; N, 12.48; Mn, 30.35. Yield: 20%. IR (ν_{max}/cm^{-1}, KBr pellet): ν(N≡N−N) 2057(vs), $\nu(C{=}N)_{pyridyl}$ 1598(vs).

Procedure 2. An alternative preparation of the complex was done according to the following procedure. A 25 mmol portion of $MnCl_2\cdot 4H_2O$ and 5 mmol of sodium azide were dissolved in 30 mL of methanol, and the mixture was stirred for 30 min. Another mixture of 10 mmol of di-2-pyridyl ketone and 30 mmol of sodium hydroxide dissolved in 20 mL of methanol was stirred for 1 h. The second solution was added into the first one over a period of 15 min. The mixture became dark brown after 1 h of stirring. A red/black crystalline product was obtained by slow evaporation of the mother liquid over a few days. Yield: 60%. These crystals have been characterized as having the formula of **1**.

$[Mn^{II}_4Mn^{III}_{22}(pdol)_{12}(\mu_3\text{-}OCH_3)_{12}(\mu_3\text{-}O)_6(\mu_4\text{-}O)_{10}(OH)_2(H_2O)(OCH_3)_3]\cdot ClO_4\cdot 5CH_3OH$ (2). A mixture of 10 mmol of di-2-pyridyl ketone and 20 mmol of sodium hydroxide dissolved in 20 mL of methanol was stirred for 1 h. A 25 mmol portion of $Mn(ClO_4)_2\cdot 6H_2O$ dissolved in 100 mL of methanol was added dropwise over a period of 30 min, and the mixture was stirred for 4 h. The mixture became dark black-brown after 2 h of stirring. The reaction mixture was filtered, and the filtrate was left for slow evaporation. A red/black crystalline product was obtained over a few days, and the crystals were suitable for X-ray crystal structure determination. These crystals have been characterized as having the formula $C_{152}H_{169}ClMn_{26}N_{24}O_{69}$ (fw = 4799.97). Analytical data: found C, 41.50; H, 3.30; N, 7.00; requires C 41.38; H, 3.45; N, 6.85; Mn, 29.18. Yield: 70%. IR (ν_{max}/cm^{-1}, KBr pellet): $\nu(C{=}N)_{pyridyl}$ 1598(vs), $\nu(Cl{-}O)_{asym}$ 1100(vs), $\nu(Cl{-}O)_{sym}$ 1075(vs), δ(Cl−O) 625(s). UV−vis [λ (ϵ, $M^{-1}\cdot cm^{-1}$), DMF]: 362 (4425), 500(sh) (1700), 585(sh) (800).

Caution! *Organic perchlorate salts are potentially explosive. These complexes should be synthesized only in small quantities and handled with utmost care.*

Physical Measurements. Variable-temperature, variable-field dc magnetization measurements were performed using a vibrating sample magnetometer (VSM), which was coupled to a He^{III} refrigeration system and capable of temperatures as low as 0.55 K. A water-cooled resistive Bitter magnet was used to provide continuous magnetic field sweeps between 0 and 30 T. Isothermal magnetization measurements were performed between 0.6 and 4.5 K. The VSM measurements were conducted at the National High Magnetic Field Laboratory at Florida State University. Isofield variable-temperature dc magnetic susceptibility measurements were performed at 0.25 T on a Quantum Design MPMS SQUID magnetometer from 2 to 300 K. All dc magnetic susceptibility data were collected on powdered samples suspended in eicosane to prevent torquing of the sample at high applied dc magnetic fields. Alternating current magnetic susceptibility measurements were made on powdered samples in an ac drive field operating at frequencies between 100 and 5000 Hz with zero applied dc magnetic field. A

(73) Milios, C. J.; Raptopoulou, C. P.; Terzis, A.; Lloret, F.; Vicente, R.; Perlepes, S. P.; Escuer, A. *Angew. Chem., Int. Ed.* **2004**, *43*, 210.
(74) Koizumi, S.; Nihei, M.; Nakano, M.; Oshio, H. *Inorg. Chem.* **2005**, *44*, 1208.
(75) Boskovic, C.; Wernsdorfer, W.; Folting, K.; Huffman, J. C.; Hendrickson, D. N.; Christou, G. *Inorg. Chem.* **2002**, *41*, 5107.
(76) Tasiopoulos, A. J.; Wernsdorfer, W.; Moulton, B.; Zaworotko, M. J.; Christou, G. *J. Am. Chem. Soc.* **2003**, *125*, 15274.
(77) Brechin, E. K.; Soler, M.; Christou, G.; Helliwell, M.; Teat, S. J.; Wernsdorfer, W. *Chem. Commun.* **2003**, 1276.
(78) Brechin, E. K.; Soler, M.; Davidson, J.; Hendrickson, D. N.; Parsons, S.; Christou, G. *Chem. Commun.* **2002**, 2252.
(79) Brechin, E. K.; Soler, M.; Christou, G.; Davidson, J.; Hendrickson, D. N.; Parsons, S.; Wernsdorfer, W. *Polyhedron* **2003**, *22*, 1771.
(80) Sun, Z.; Grant, C. M.; Castro, S. L.; Hendrickson, D. N.; Christou, G. *Chem. Commun.* **1998**, 721.
(81) Barra, A. L.; Debrunner, P.; Gatteschi, D.; Schulz, C. E.; Sessoli, R. *Europhys. Lett.* **1996**, *35*, 133.
(82) Bouwen, A.; Caneschi, A.; Gatteschi, D.; Goovaerts, E.; Schoemaker, D.; Sorace, L.; Stefan, M. *J. Phys. Chem. B* **2001**, *105*, 2658.
(83) Cornia, A.; Fabretti, A. C.; Garrisi, P.; Mortalo, C.; Bonacchi, D.; Gatteschi, D.; Sessoli, R.; Sorace, L.; Wernsdorfer, W.; Barra, A. L. *Angew. Chem., Int. Ed.* **2004**, *43*, 1136.
(84) Yang, E.; Hendrickson, D. N.; Wernsdorfer, W.; Nakano, M.; Zakharov, L. N.; Sommer, R. D.; Rheingold, A. L.; Ledezma-Gairaud, M.; Christou, G. *J. Appl. Phys.* **2002**, *91*, 7382.
(85) Murrie, M.; Teat, S. J.; Stoecki-Evans, H.; Gudel, H. *Angew. Chem., Int. Ed.* **2003**, *42*, 4653.
(86) Ochsenbein, S. T.; Murrie, M.; Rusanov, E.; Stoeckli-Evans, H.; Sekine, C.; Gudel, H. *Inorg. Chem.* **2002**, *41*, 5133.
(87) Andres, H.; Basler, R.; Blake, A. J.; Cadiou, C.; Chaboussant, G.; Grant, C. M.; Gudel, H.; Murrie, M.; Parsons, S.; Paulsen, C.; Semadini, F.; Villar, V.; Wernsdorfer, W.; Winpenny, R. E. P. *Chem. Eur. J.* **2002**, *8*, 4867.
(88) Osa, S.; Kido, T.; Matsumoto, N.; Re, N.; Pochaba, A.; Mrozinski, J. *J. Am. Chem. Soc.* **2004**, *126*, 420.
(89) Zaleski, C. M.; Depperman, E. C.; Kampf, J. W.; Kirk, M. L.; Pecoraro, V. L. *Angew. Chem., Int. Ed.* **2004**, *43*, 3912.
(90) Mishra, A.; Wernsdorfer, W.; Abboud, K. A.; Christou, G. *J. Am. Chem. Soc.* **2004**, *126*, 15648.

Table 1. Crystallographic Data for **2**

chemical formula	$C_{152}H_{165}ClMn_{26}N_{24}O_{69}$
formula weight	4895.97
space group	*P*31*c* (no. 159)
a	20.2656(12) Å
b	20.2656(12) Å
c	33.203(4) Å
α	90°
β	90°
γ	120°
temperature	118(2) K
λ	0.71073 Å
ρ_{calc}	1.377 mg/m^3
μ	1.419 mm^{-1}
volume	11809.4(16) Å^3
Z	2
R_1[a,b]	0.0329
wR_2[a,c]	0.0976

[a] 18 317 unique data with $I > 2\sigma(I)$. [b] $R_1 = \sum(||F_o| - |F_c||)/\sum|F_o|$. [c] $wR_2 = [\sum[w(F_o^2 - F_c^2)^2]/\sum[w(F_o)^2]]^{1/2}$; $w = 1/[\sigma^2(F_o^2) + (mp)^2 + np]$; $p = [\max(F_o^2,0) + 2F_c^2]/3$ (*m* and *n* are constants); $\sigma = [\sum[w(F_o^2 - F_c^2)^2]/(n - p)]^{1/2}$.

Quantum Design MPMS SQUID instrument was used in the 2−10 K range with a 3.5 G ac drive field, and a custom ac susceptometer at the National High Magnetic Field Laboratory at Florida State University was used in the 0.3−6 K range with a 50 G ac drive field. All solid samples were packed into gelatin capsules, and all magnetic susceptibility values were corrected with Pascal's constants. A ∼1 mM solution of **2** in DMSO was sealed in a quartz tube and used for frozen solution ac magnetic susceptibility measurements in the 2−10 K range. Infrared spectra (200−4000 cm^{-1}) were recorded on a Perkin-Elmer FT-IR 1650 spectrometer, with samples prepared as KBr pellets. Elemental analyses were performed on a Perkin-Elmer 240B elemental analyzer. UV−vis spectra were recorded on a Shimadzu-160A dual beam spectrophotometer.

X-ray Crystallography. Crystals of **2** were obtained as described above. The crystal was mounted on a standard Bruker SMART CCD-based X-ray diffractometer equipped with an LT-2 low-temperature device and a normal focus Mo-target X-ray tube ($\lambda = 0.71073$ Å) operated at 2000 W power (50 kV, 40 mA). The X-ray intensities were measured at 118(2) K; the detector was placed at a distance 4.954 cm from the crystal. A total of 3297 frames were collected with a scan width of 0.2° in *ω* with an exposure time of 30 s/frame. The frames were integrated with the Bruker SAINT software package with a narrow frame algorithm. The integration of the data yielded a total of 138 757 reflections to a maximum 2θ value of 56.76°, of which 19 533 were independent and 18 317 were greater than $2\sigma(I)$. The final cell constants were based on the *xyz* centroids of 7869 reflections above $10\sigma(I)$. Analysis of the data showed negligible decay during data collection; the data were processed with SADABS and corrected for absorption. The structure was solved and refined with the Bruker SHELXTL (version 5.10) software package. The contributions of lattice methanol and water solvates were included as diffuse scattering by use of the SQUEEZE routing of the PLATON program suite. All non-hydrogen atoms were refined anisotropically with the hydrogen placed in idealized positions. Full-matrix least-squares refinement based on F^2 converged at $R_1 = 0.0329$ and $wR_2 = 0.0972$ [based on $I > 2\sigma(I)$]; $R_1 = 0.0361$ and $wR_2 = 0.0994$ for all data. Experimental parameters and crystallographic data are provided in Table 1. Important bond distances and angles are provided in Tables 2 and 3, respectively.

Results

Synthesis. The synthesis of the manganese metallacryptates **1** and **2** has been achieved through similar routes. For **1** the synthesis was via the aerial redox reaction of $MnCl_2$ with di-2-pyridyl ketone and NaN_3 in an alkaline methanolic solution (Scheme 1). Compound **1** is a red-black crystalline solid, and

Scheme 1

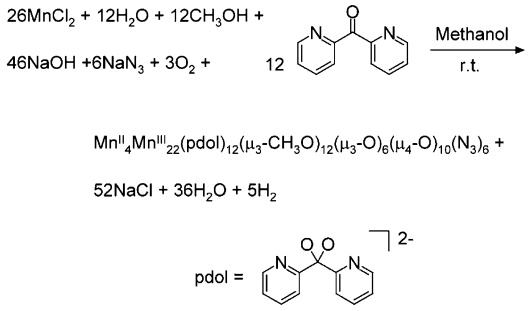

it is only sparingly soluble in DMSO. The synthesis of **2** proceeded via the aerial redox reaction of $Mn(ClO_4)_2$ with di-2-pyridyl ketone in an alkaline methanolic solution (Scheme 2). Compound **2** is a red-black crystalline solid, and it is soluble in DMSO and 1:1 electrolyte in DMF or DMSO.

Table 2. Selected Bond Distances (Å) for **2**

Mn(1)−O(4)	1.875(2)	Mn(3)−O(5)	2.133(3)	Mn(6)−O(10)	1.884(2)	Mn(8)−O(18b)	2.269(2)
Mn(1)−O(2)	1.907(2)	Mn(3)−N(3)	2.179(3)	Mn(6)−O(14)	1.904 (2)	Mn(8)−O(20)	2.282(2)
Mn(1)−O(1)	1.907(8)	Mn(3)−N(2)	2.193(3)	Mn(6)−O(8)	1.905(2)	Mn(9)−O(18)	1.988(2)
Mn(1)−O(15)	1.957(19)	Mn(4)−O(4)	1.871(2)	Mn(6)−O(13)	1.959(2)	Mn(9)−O(18a)	1.988(2)
Mn(1)−O(16)	2.281(2)	Mn(4)−O(14)	1.904 (2)	Mn(6)−O(17)	2.252(2)	Mn(9)−O(18b)	1.988(2)
Mn(1)−O(16a)	2.309(2)	Mn(4)−O(6)	1.914(2)	Mn(6)−O(18)	2.316(2)	Mn(9)−O(13)	2.029(2)
Mn(2)−O(2)	2.238(2)	Mn(4)−O(15)	1.960(2)	Mn(7)−O(11)	1.882(2)	Mn(9)−O(13a)	2.029(2)
Mn(2)−O(2a)	2.238(2)	Mn(4)−O(17)	2.272(2)	Mn(7)−O(9)	1.897(2)	Mn(9)−O(13b)	2.028(2)
Mn(2)−O(2b)	2.238(2)	Mn(4)−O(20a)	2.307(2)	Mn(7)−O(10)	1.908(2)	Mn(10)−O(20a)	1.939(2)
Mn(2)−O(1)	2.392(3)	Mn(5)−O(6)	2.224(2)	Mn(7)−O(19)	2.071(3)	Mn(10)−O(15a)	1.957(2)
Mn(2)−N(1)	2.458(2)	Mn(5)−O(8)	2.226(2)	Mn(7)−N(6)	2.234(3)	Mn(10)−O(16a)	1.981(2)
Mn(2)−N(1a)	2.458(2)	Mn(5)−O(12a)	2.231(2)	Mn(7)−N(7)	2.243(3)	Mn(10)−O(13a)	2.011(2)
Mn(2)−N(1b)	2.458(2)	Mn(5)−O(14)	2.386(2)	Mn(8)−O(10)	1.882 (2)	Mn(10)−O(17a)	2.050(2)
Mn(3)−O(3)	1.866(2)	Mn(5)−N(5)	2.421(2)	Mn(8)−O(12)	1.905(2)	Mn(10)−O(15)	2.089(2)
Mn(3)−O(7)	1.886(2)	Mn(5)−N(8a)	2.437(2)	Mn(8)−O(14b)	1.907(2)		
Mn(3)−O(4)	1.911(2)	Mn(5)−N(4)	2.465(2)	Mn(8)−O(13)	1.956(2)		
Mn(1)−Mn(4)	2.933(6)	Mn(4)−Mn(6)	3.208(6)	Mn(9)−Mn(6a)	3.108(5)	Mn(10)−Mn(4a)	3.076(6)
Mn(1)−Mn(10b)	3.091(6)	Mn(4)−Mn(8a)	3.234(6)	Mn(9)−Mn(8b)	3.117(4)	Mn(10)−Mn(1a)	3.091(6)
Mn(1)−Mn(10)	3.118(6)	Mn(6)−Mn(8)	2.935(6)	Mn(9)−Mn(8)	3.117(5)	Mn(10)−Mn(8a)	3.100(6)
Mn(1)−Mn(1b)	3.225(7)	Mn(6)−Mn(9)	3.108(4)	Mn(9)−Mn(8a)	3.117(5)	Mn(10)−Mn(6a)	3.117(6)
Mn(1)−Mn(1a)	3.226(7)	Mn(6)−Mn(10b)	3.118(6)	Mn(8)−Mn(10b)	3.100(6)		
Mn(4)−Mn(10b)	3.076(6)	Mn(6)−Mn(8a)	3.235(6)	Mn(8)−Mn(4b)	3.234(6)		
Mn(4)−Mn(10)	3.145(6)	Mn(9)−Mn(6b)	3.108(4)	Mn(8)−Mn(6b)	3.235(6)		

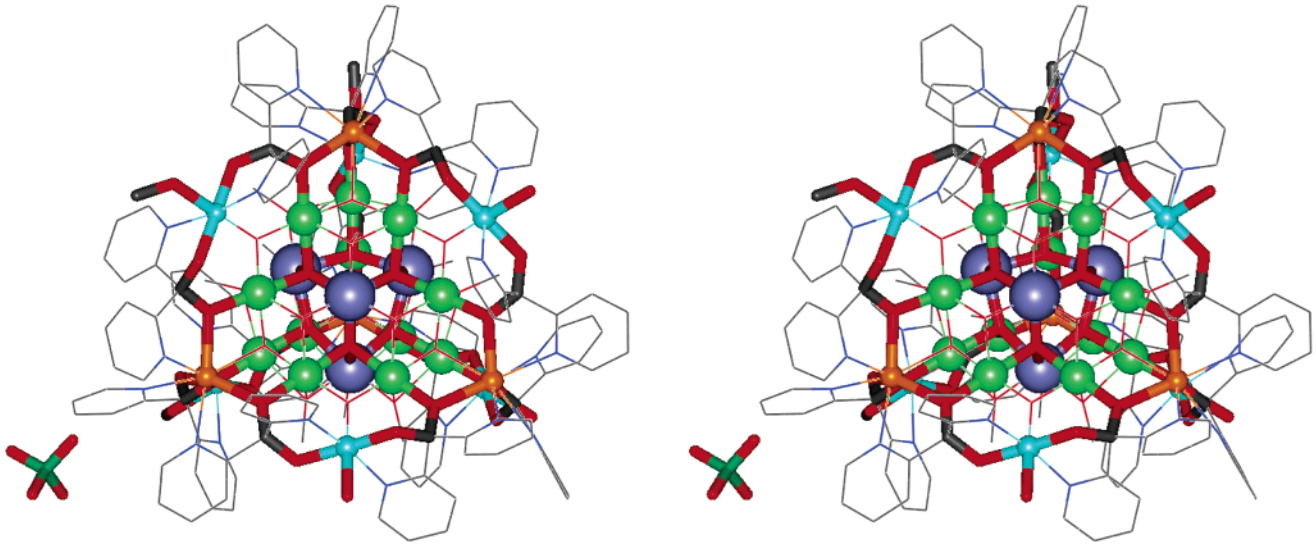

Figure 1. Stereoview of the X-ray crystal structure of **2**. The core and ring connectivity are highlighted with thick tubes. Color scheme: orange spheres, Mn2 and Mn5; green spheres, Mn3 and Mn7; aqua spheres, Mn1, Mn4, Mn6, and Mn8; navy blue spheres, Mn9 and Mn10; gray tubes, carbon; red tubes, oxygen; dark green tube, chlorine. Hydrogen atoms and lattice solvent are omitted for clarity.

Table 3. Selected Bond Angles (deg) for **2**

Mn(1a)−O(1)−Mn(1b)	115.52(7)	Mn(8)−O(13)−Mn(6)	97.14(9)	Mn(10b)−O(15)−Mn(10)	141.49(10)
Mn(1a)−O(1)−Mn(1)	115.51(7)	Mn(8)−O(13)−Mn(10b)	102.78(10)	Mn(4)−O(15)−Mn(10)	101.90(9)
Mn(1b)−O(1)−Mn(1)	115.51(7)	Mn(6)−O(13)−Mn(10b)	103.48(10)	Mn(10b)−O(16)−Mn(1)	92.70(8)
Mn(1a)−O(1)−Mn(2)	102.41(9)	Mn(8)−O(13)−Mn(9)	102.93(10)	Mn(10b)−O(16)−Mn(1b)	92.93(8)
Mn(1b)−O(1)−Mn(2)	102.41(9)	Mn(6)−O(13)−Mn(9)	102.41(10)	Mn(1)−O(16)−Mn(1b)	89.29(7)
Mn(1)−O(1)−Mn(2)	102.41(9)	Mn(10b)−O(13)−Mn(9)	140.55(10)	Mn(10b)−O(17)−Mn(6)	92.77(8)
Mn(1)−O(2)−Mn(2)	108.28(9)	Mn(6)−O(14)−Mn(4)	114.76(9)	Mn(10b)−O(17)−Mn(4)	90.58(8)
Mn(4)−O(4)−Mn(1)	103.08(9)	Mn(6)−O(14)−Mn(8a)	116.17(9)	Mn(6)−O(17)−Mn(4)	90.31(7)
Mn(4)−O(4)−Mn(3)	128.68(11)	Mn(4)−O(14)−Mn(8a)	116.13(9)	Mn(9)−O(18)−Mn(8a)	93.90(8)
Mn(1)−O(4)−Mn(3)	128.23(10)	Mn(6)−O(14)−Mn(5)	102.06(8)	Mn(9)−O(18)−Mn(6)	92.12(8)
Mn(4)−O(6)−Mn(5)	107.61(9)	Mn(4)−O(14)−Mn(5)	101.84(8)	Mn(8a)−O(18)−Mn(6)	89.73(7)
Mn(6)−O(8)−Mn(5)	108.10(9)	Mn(8a)−O(14)−Mn(5)	102.58(8)	Mn(10b)−O(20)−Mn(8)	94.19(8)
Mn(8)−O(10)−Mn(6)	102.37(9)	Mn(1)−O(15)−Mn(10b)	104.31(9)	Mn(10b)−O(20)−Mn(4b)	95.21(8)
Mn(8)−O(10)−Mn(7)	128.99(11)	Mn(1)−O(15)−Mn(4)	96.98(8)	Mn(8)−O(20)−Mn(4b)	89.60(7)
Mn(6)−O(10)−Mn(7)	128.63(11)	Mn(10b)−O(15)−Mn(4)	103.47(9)		
Mn(8)−O(12)−Mn(5b)	108.57(8)	Mn(1)−O(15)−Mn(10)	100.81(9)		

Scheme 2

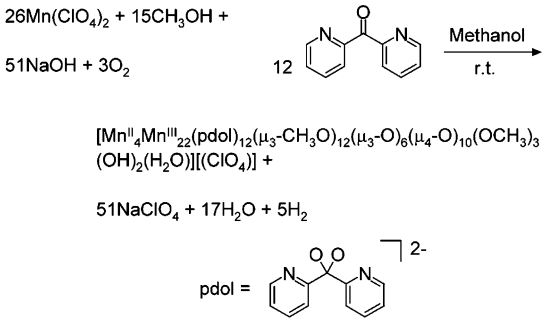

Structural Description. The structure of **1** has been previously described.[23] Complex **2** (Figure 1) can conceptually be broken into two units. One portion is an outer metallacryptand that encapsulates the second portion, an inner manganese oxide core. The metallacryptand (Mn2, Mn3, Mn5, and Mn7) is composed of manganese ions and pdol^{2-} ligands and wraps around a $\{Mn_{16}(O^{2-})_{12}(MeO^{-})_{16}\}$ core (Mn1, Mn4, Mn6, Mn8, Mn9, and Mn10). The strands of the metallacryptand are pinned down by four Mn^{II} ions (Mn2 and Mn5), which are connected by pdol−Mn^{III}−pdol repeat units (Mn3 and Mn7). The metallacryptand has an overall adamantoid topology,[91,92] forming a [4]-metallacryptand.

Mn2 and Mn5 are chemically equivalent centers with slight differences in ligand bond distances that form the hinges of the metallacryptand. Mn2 and Mn5 are both seven-coordinate centers. They are surrounded by portions from three different pdol^{2-} ligands. Three pyridyl nitrogen atoms (N1, N1a, N1b for Mn2; N5, N5, N8 for Mn5) and three μ-oxygen atoms (O2, O2a, O2b for Mn2; O6, O8, O12a for Mn5) form an octahedral polyhedron around the manganese center. The seventh ligand, a μ_4-oxide oxygen atom (O1 for Mn2; O14 for Mn5), caps one face of the polyhedron. The μ_4-oxide oxygen atom forms a part of the manganese oxide core and links the metallacryptand to the core. Based on the average Mn−N/O bond distances of 2.36 Å (Mn2) and 2.34 Å (Mn5), the assigned oxidation state is 2+. For comparison, a seven-coordinate Mn^{III} ion has an average bond length of 2.13 Å.[93]

Mn3 and Mn7 play a role in the strands of the metallacryptand. Mn3 and Mn7 are both six-coordinate but differ in the bound anion. Mn3 is surround by two pyridyl nitrogen atoms (N2, N3) and two oxygen atoms (O3, O7) from two pdol^{2-} ligands and a μ_3-oxide oxygen atom (O4) from the core. The coordination sphere is completed by an oxygen atom (O5) from either a hydroxide anion or a water molecule. Two of the three crystallographically equivalent Mn3 ions are bound to a hydroxide anion, and the third is bound to a water molecule.

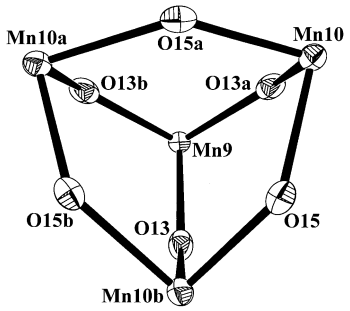

Figure 2. ORTEP diagram of the Mn_4 core of **2**. Thermal ellipsoids are at 50% probability.

However, the three coordinated species are disordered over all three positions, so it is not possible to determine the exact location of the water and hydroxide species. Mn7 is also surround by two pyridyl nitrogen atoms (N6, N7) and two oxygen atoms (O9, O11) from two $pdol^{2-}$ ligands and a μ_3-oxide oxygen atom (O10) from the core. The coordination sphere is completed by an oxygen atom (O19) from a methoxide. All three Mn7 ions are bound to methoxide oxygen atoms. One could argue that Mn3 is bound to three hydroxides and the Mn7 is bound to two methoxides and one methanol (the opposite case of what is presented), but based on crystallographic data we are confident in our assignment. The average Mn3−$O_{hydroxide/water}$ bond is 2.13 Å, while that of the average Mn7−$O_{methoxide}$ is 2.07 Å. On the basis of average Mn−N/O bond distances, Mn3 (2.02 Å) and Mn7 (2.04 Å) are assigned an oxidation state of 3+. In addition, both Mn3 and Mn7 contain a Jahn−Teller axis along the Mn−$N_{pyridyl}$ bonds, with average bond distances of 2.19 Å (Mn3) and 2.24 Å (Mn7).

Twelve manganese ions of the $\{Mn_{16}(O^{2-})_{12}(MeO^{-})_{16}\}$ core consist of the chemically equivalent Mn1, Mn4, Mn6, and Mn8 and are directly bonded to the metallacryptand. The coordination environment is composed of one μ-oxygen atom (O2 for Mn1; O6 for Mn4; O8 for Mn6; O12 for Mn8) from the $pdol^{2-}$ ligands, two μ_3-methoxide oxygen atoms (O16, O16a for Mn1; O17, O20a for Mn4; O17, O18 for Mn6; O18b, O20 for Mn8), one μ_3-oxide oxygen atom (O4 for Mn1; O4 for Mn4; O10 for Mn6; O10 for Mn8), and two μ_4-oxide oxygen atoms (O1, O4 for Mn1; O14, O15 for Mn4; O13, O14 for Mn6; O13, O14b for Mn8). An average Mn−N/O distance (Mn1, 2.04 Å; Mn4, 2.04 Å; Mn6, 2.04 Å; Mn8, 2.03 Å) and Jahn−Teller axes along the Mn−$O_{methoxide}$ bond (average Mn−$O_{methoxide}$ bond distances: Mn1, 2.27 Å; Mn4, 2.29 Å; Mn6, 2.28 Å; Mn8, 2.28 Å) support an assigned oxidation state of 3+. The four remaining manganese ions (Mn9 and Mn10) (Figure 2) comprise the rest of the core and are isolated from the metallacryptand. These manganese centers (Mn9 and Mn10) are connected to the outer 12 manganese core ions via oxygen atom bridges. Each manganese ion is six-coordinate and surrounded by three μ_3-methoxide oxygen atoms (O18, O18a, O18b for Mn9; O16a, O17a, O20a for Mn10) and three μ_4-oxide oxygen atoms (O13, O13a, O13b for Mn9; O13a, O15, O15a for Mn10). These centers are assigned a 3+ oxidation state on the basis of average bond distances of 2.01 Å (Mn9) and 2.00 Å (Mn10).

(91) Saalfrank, R. W.; Stark, A.; Peters, K.; von Schnering, H. G. *Angew. Chem., Int. Ed. Engl.* **1988**, *27*, 851.
(92) Saalfrank, R. W.; Stark, A.; Bremer, M.; Hummel, H.-U. *Angew. Chem., Int. Ed. Engl.* **1990**, *29*, 311.
(93) Sreerama, S. G.; Pal, S. *Inorg. Chem.* **2002**, *41*, 4843.

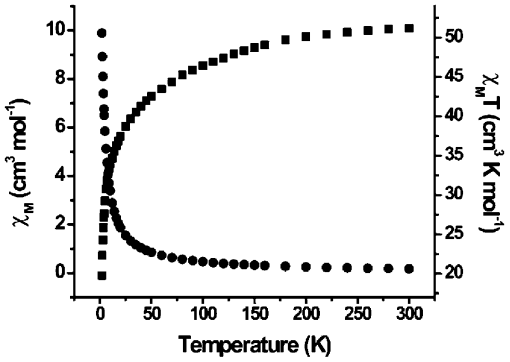

Figure 3. Variable-temperature dc magnetic susceptibility data for **2**. ●, χ_M; ■, $\chi_M T$.

In the solid state along the *c* axis, **2** is hexagonal close-packed. The arrangement of the triangles gives the appearance of a hexagonal channel running through the solid.

Variable-Temperature DC Magnetic Susceptibility. Variable-temperature dc magnetic susceptibility measurements were collected on a powdered sample of **2** suspended in eicosane from 2 to 300 K at 0.25 T (Figure 3). The room-temperature χT value for **2** is 51.2 cm^3 K mol^{-1}, which is markedly lower than the spin-only value for a $Mn^{II}_4Mn^{III}_{22}$ system (83.5 cm^3 K mol^{-1}). Upon decreasing the temperature, χT decreases, confirming the overall antiferromagnetic interaction. Taken together, these data indicate that overall antiferromagnetic interactions dominate in the cluster. Finally, the χT value drastically decreases at temperatures below ~15 K due to a combination of antiferromagnetic exchange, zero-field splitting, and Zeeman effects. Although antiferromagnetic pairwise exchange interactions dominate in **2**, the χT value is still large at 2 K (19.8 cm^3 K mol^{-1}), indicating a relatively high-spin ground state for the cluster.

Variable-Field DC Magnetization. Variable-field magnetization measurements were performed on a vibrating-sample magnetometer in applied magnetic fields between 0 and 30 T. Powdered samples were suspended in eicosane to prevent crystallite torquing at high applied dc magnetic fields. Magnetization measurements for **1** at 0.6 and 1.6 K reveal that the magnetization does not saturate at 30 T (Figure S1), and the data collected at 0.6 and 1.6 K are essentially superimposable. At 30 T and 0.6 K, the value of the magnetization is approximately 143 000 cm^3 G mol^{-1}. The reduced magnetization curves of **1** indicate a zero-field splitting of the ground spin state (Figure 4). Complex **2** displays similar saturation magnetization behavior at 0.6 and 1.6 K (Figure S2), and the magnetization at 30 T and 0.6 K is approximately 137 000 cm^3 G mol^{-1}. The reduced magnetization curves for **2** also indicate the presence of a zero-field splitting of the ground spin state (Figure 5). Interestingly, the magnetization values at 4.3 K are noticeably lower than those obtained at either 0.6 and 1.6 K, indicating that a different subset of magnetic states are being populated at higher temperatures. As in the case of **1**, the magnetization does not saturate. These are important observations, as nonsaturating magnetization values in large cluster SMMs have been interpreted as resulting from a high density of states being thermally populated at low temperatures, a substantial temperature-independent paramagnetism (TIP) resulting from field-induced mixing of higher energy states which

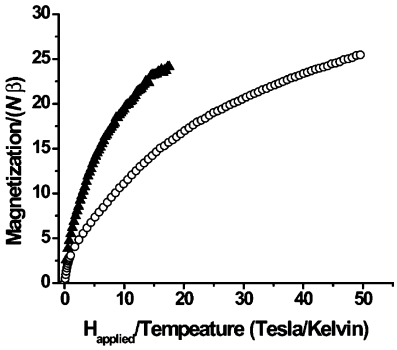

Figure 4. Reduced magnetization data for **1**. ○, 0.6 K; ▲, 1.6 K. *N* is Avogadro's number, and β is the Bohr magneton.

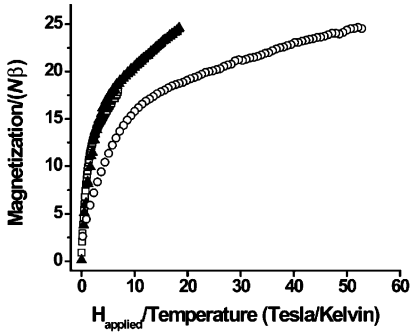

Figure 5. Reduced magnetization data for **2**. ○, 0.6 K; ▲, 1.6 K; □, 4.3 K. *N* is Avogadro's number, and β is the Bohr magneton.

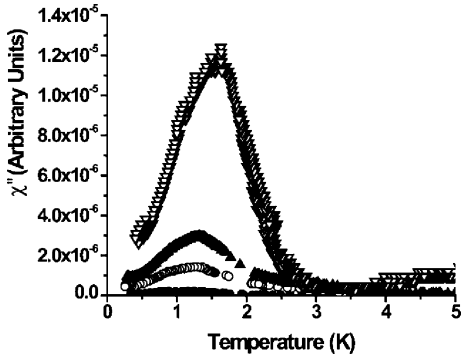

Figure 6. Variable-temperature imaginary component of **1**. ▽, 5000 Hz; ▲, 1000 Hz; ○, 500 Hz; ●, 100 Hz.

are not thermally populated at the measurement temperatures, or a combination of both.[23,59,65]

Variable-Temperature AC Magnetic Susceptibility. Variable-temperature ac magnetic susceptibility data were collected on either a Quantum Design MPMS SQUID magnetometer or the NHMFL ac susceptometer at Florida State University. Measurements were conducted on powdered samples for both **1** and **2**. Complex **1** shows frequency-dependent behavior in the out-of-phase signal. As the frequency is decreased from 5000 to 100 Hz, the blocking temperature (maximum peak height) decreases from 1.5 to 1.0 K (Figure 6), a behavior suggestive of single-molecule magnet behavior. There is also a decrease in the in-phase signal (Figure S3). Additional measurements were performed on a MPMS system in order to obtain quantitative values for the ac susceptibility. The ground spin state of the complex can be approximated from an extrapolation of the in-phase signal in zero applied dc magnetic field.[94] The extrapolated value, as $T \rightarrow 0$, of the $\chi'T$ product for **1** is

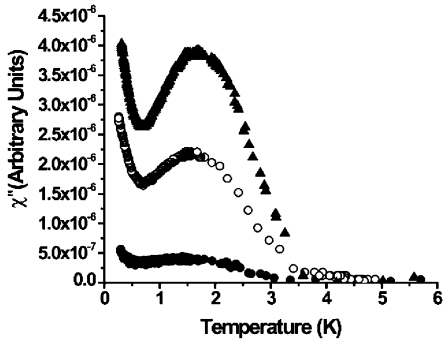

Figure 7. Variable-temperature imaginary component of **2**. ▲, 1000 Hz; ○, 500 Hz; ●, 100 Hz.

approximately 13 cm^3 K mol^{-1} using only the data at temperatures prior to the divergence of χ' and χ''. The extrapolated $\chi'T$ product indicates either an $S = 4$ or $S = 5$ ground state (Figures S4 and S5) for **1**, though this has not been confirmed with other measurements and can only be considered approximate. Complex **2** possesses a similar in-phase and out-of-phase ac behavior in the 1000 to 100 Hz range (Figures 7 and S6). Extrapolation of the high-temperature $\chi'T$ data for **2** yields a value of approximately 27 cm^3 K mol^{-1}, which indicates a spin ground state of $S = 7$ (Figures S7 and S8). To confirm that the ac susceptibility data derive from single-molecule magnet behavior, and not cooperative magnetism, identical ac magnetic susceptibility studies were performed on a ~1 mM frozen solution of **2** in DMSO (2−10 K). A frequency-dependent out-of-phase magnetic susceptibility signal was observed for **2** (Figures S8 and S9), clearly indicating that the solid-state magnetic behavior is intrinsic to the cluster and devoid of cooperative or intercluster effects.

At the maximum in the χ'' vs *T* data, the ac angular frequency (ω) is equal to the magnetization relaxation rate ($1/\tau$), and $\omega\tau = 1$.[95] Fitting these data to the Arrhenius equation allows one to determine the energy barrier to magnetization relaxation:

$$1/\tau = 1/\tau_o \exp(-U_{eff}/kT) \quad (1)$$

$$\ln(1/\tau) = -U_{eff}/kT + \ln(1/\tau_o) \quad (2)$$

where *k* is the Boltzmann constant, *T* is the temperature, U_{eff} is the energy barrier to magnetization relaxation, and τ_o[96] is the pre-exponential factor. For **1** U_{eff} is determined to be 16.5 ± 0.7 K (11.5 ± 0.5 cm^{-1}) and $1/\tau_o = 2.2 \times 10^9$ s^{-1} (Figure S10), while for **2** U_{eff} is 36.2 ± 2.0 K (25.1 ± 1.4 cm^{-1}) and $1/\tau_o = 1.9 \times 10^{13}$ s^{-1} (Figure S11).

Discussion

Complexes **1** and **2** are very similar in the overall topology of the metallacryptand strands and their connectivity to the manganese oxide core. The most important structural differences are the nature of the anion bound to the metallacryptand Mn^{III} centers and the geometry of the tetranuclear manganese oxide core that is isolated from the metallacryptand. It is evident that the nature of the anion directly affects the geometry of this inner

(94) Chakov, N. E.; Wernsdorfer, W.; Abboud, K. A.; Christou, G. *Inorg. Chem.* **2004**, *43*, 5919.
(95) Novak, M. A.; Sessoli, R. In *Quantum Tunneling of Magnetization—QTM '94*; Gunther, L., Barbara, B., Eds.; Kluwer Academic Publishers: Dordrecht, The Netherlands, 1995; p 171.
(96) Kilcoyne, S. H.; Cywinski, R. *J. Magn. Mater.* **1995**, *140−144*, 1466.

tetranuclear Mn core, resulting in a T_d core geometry for **1** and a C_3 core geometry for **2**. Due to the lower symmetry of **2**, there are more crystallographically unique manganese ions in the molecule compared to **1** even though the number of chemically equivalent manganese ions is the same. In place of the azide anions bound to the Mn^{III} metallacryptand strands in **1**, the strand Mn^{III} ions of **2** have bound hydroxide anions, water molecules, and methoxide anions. In addition, to compensate for the positive charge on **2**, one perchlorate anion is unbound and located in the lattice. This perchlorate anion is nearest to Mn5. This leads to another fundamental difference between these two complexes. The metallacryptate of **1** is chemically neutral, while the metallacryptate of complex **2** is a cation. Finally, the three-dimensional packing of the two compounds in the crystal lattice is different. Complex **1** packs in a cubic closed-packed arrangement, while **2** packs in a hexagonal closed-packed structure with a hexagonal channel running through the solid. These differences in symmetry, electronic structure, and solid-state packing are all potential candidates for modulating the observed magnetic properties of these two complexes.

The dc magnetic susceptibility results show that the high-temperature χT values for **2** are lower than those of complex **1** (at 300 K: **1**, 70.3 cm^3 K mol^{-1}; **2**, 51.2 cm^3 K mol^{-1}) in an applied magnetic field of 0.25 T, and this can be interpreted to indicate that the overall antiferromagnetic interactions in **2** are stronger than those of **1**. The sharp decrease in the χT value at low temperatures for **1** and **2** is likely due to a combination of Zeeman effects, zero-field splitting, and the overall antiferromagnetic exchange coupling scheme. Unfortunately, the large number of Mn ions, the complex nature of the structures, and the presence of multiple magnetic exchange pathways in **1** and **2** preclude a determination of the individual pairwise exchange interaction parameters, J_i, for these interesting clusters.

In the previous report on **1**,[23] the magnetization of the sample did not saturate at applied magnetic field as high as 5.5 T, and this precluded a definitive assignment of the ground-state spin. In an additional effort to saturate the magnetization of **1** and **2**, variable-temperature magnetization studies were conducted at applied fields as high as 30 T. Interestingly, the magnetization of **1** and **2** still does not saturate, and at the highest applied fields the magnetization increases linearly with field. This could result from field level crossings that occur as a result of a high density of magnetic states or a sizable temperature-independent paramagnetism, which is a result of field-induced mixing of specific excited spin states with the ground spin state. Since antiferromagnetic interactions are apparent in **1** and **2**, the zero-field ground state does not derive from states of highest spin multiplicity, S. High applied magnetic fields will result in larger m_s, components of states possessing higher spin multiplicity being stabilized relative to the zero-field ground state. Extensive level crossing is anticipated under these conditions, and in the absence of direct evidence for a large TIP, energy level crossing and a high density of states are the likely reasons saturation of the magnetization is not observed in applied fields as large as 30 T.

Complex **1** was previously shown to possess single-molecule magnet behavior,[23] and in this report both **1** and **2** display a frequency dependence of the out-of-phase magnetic susceptibility, a characteristic of SMMs. However, a critique of this observation is that the signal may be due to long-range magnetic order, glassy behavior, short-range order, or phonon bottlenecks. Therefore, analogous ac magnetic susceptibility experiments were performed on a frozen solution of **2** in DMSO in order to eliminate potential intercluster or cluster−lattice effects. Complex **2** displayed a frequency-dependent out-of-phase magnetic susceptibility in frozen solution, confirming that the magnetic behavior is intrinsic to the individual clusters in **2**, and that these Mn_{26} clusters are true SMMs. Frozen solution ac measurements could not be conducted on **1** due to the poor solubility of this species. However, the structural similarity of **1** and **2** indicates that **1** is also likely an SMM.

Table 4. Comparison of $1/\tau_o$ and U_{eff} for Large Manganese Cluster SMMs

complex	$1/\tau_o$ (s^{-1})	U_{eff} (K)	complex	$1/\tau_o$ (s^{-1})	U_{eff} (K)
Mn_{18}[62]	1.3×10^8	21.3	**1**	2.2×10^9	16
Mn_{21}[63]	1.3×10^6	11.3	**2**	1.9×10^{13}	36
Mn_{21}[64]	2.4×10^7	13.2	Mn_{26}[67]	3×10^8	15
Mn_{22}[65]	3×10^{10}	19	Mn_{30}[70]	1.5×10^8	15
Mn_{25}[66]	not reported	12	Mn_{84}[71]	1.8×10^8	18

In the previous report,[23] an effective energy barrier to magnetization relaxation could not be determined due to instrument temperature limitations. Here, the frequency dependence of the out-of-phase component of the ac susceptibility was measured at lower temperatures, and this has allowed a determination of the effective energy barrier to magnetization relaxation as well as the blocking temperature. Although the effective energy barriers to magnetization relaxation for **1** (16.5 ± 0.7 K; 11.5 ± 0.5 cm^{-1}) and **2** (36.2 ± 2.0 K; 25.1 ± 1.4 cm^{-1}) are lower than that for the original Mn_{12}OAc SMM reported in 1993 (U_{eff} = 61 K), the work presented here details how anion-induced lower symmetry effects can substantially enhance U_{eff} and the blocking temperature.[56] Large manganese clusters (Mn > 12) typically do not display a maximum in the out-of-phase ac magnetic susceptibility at temperatures above 2 K, indicative of a lower U_{eff} for these large clusters. Although U_{eff} for **1** falls within the range of reported values for large (Mn > 12) manganese clusters, U_{eff} for **2** is markedly higher and is ∼15 K higher than the largest value reported to date for an Mn > 12 SMM (Table 4).

It is of interest to understand how the lowering of the cluster symmetry can affect the SMM behavior of **2** relative to **1**, and this requires an understanding of the key structural differences between these clusters and how this relates to differences in their pairwise magnetic exchange interactions. The most prominent structural differences between **1** and **2** reside in their tetranuclear Mn cores. The tetranuclear core of **1** possesses T_d symmetry, and this is lowered appreciably, via the nature of the cluster anion, to C_3 in the tetranuclear core of **2** (Figure 8). The symmetry of the tetranuclear core of **1** results in all four of the pairwise exchange interactions in the tetranuclear T_d core of **1** being identical. Analysis of the exchange Hamiltonian for this core in zero applied magnetic field is straightforward,[97,98]

$$H = -2J(S_1 \cdot S_2 + S_1 \cdot S_3 + S_1 \cdot S_4 + S_2 \cdot S_3 + S_2 \cdot S_4 + S_3 \cdot S_4) \quad (3)$$

and yields the resultant energies for the tetranuclear $S_1 = S_2 =$

(97) Kahn, O. *Molecular Magnetism*; VCH Publishers: New York, 1993.
(98) Hatfield, W. E. In *Theory and Applications of Molecular Paramagnetism*; Boudreaux, E. A., Mulay, L. N., Eds.; Wiley-Interscience: New York, 1976; pp 381−385.

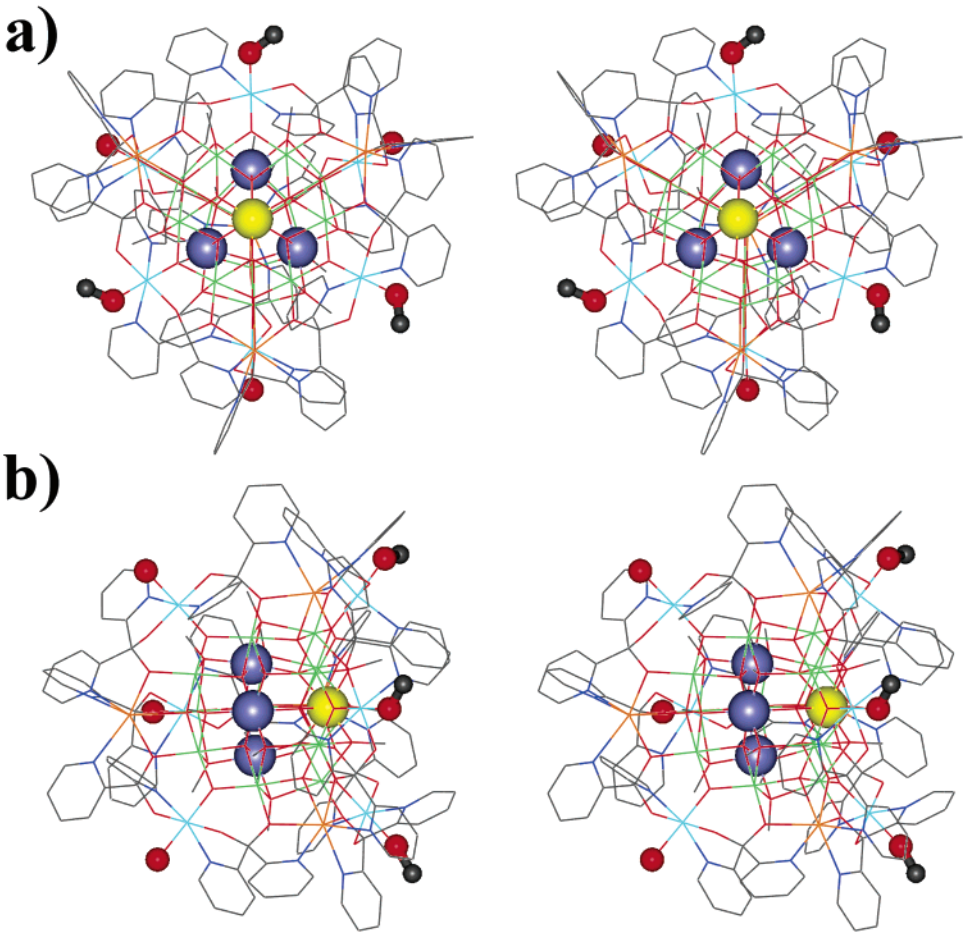

Figure 8. Stereoviews of **2** highlighting how bound anions are differentiated about the Mn9 and Mn10 core. (a) View down the pseudo-C_3 axis with methoxides above the plane of the paper and hydroxides/water below the plane of the paper. (b) Side-on view showing that all three methoxides lie to the side of Mn9 and the hydroxides/water lie to the Mn10 side. Color scheme: yellow sphere, Mn9; navy blue spheres, Mn10; gray spheres, carbon; red spheres, oxygen. Hydrogen atoms, perchlorate anion, and lattice solvent are omitted for clarity.

$S_3 = S_4 = S_i = 2$; $S = S_1 + S_2 + S_3 + S_4$ cluster,

$$E(S) = -J[S(S+1) - 4S_i(S_i+1)] \quad (4)$$

Under the assumption of dominant antiferromagnetic pairwise exchange interactions in the tetrahedral cluster, this yields an $S = 0$ ground state for **1**. The situation is quite different for the tetranuclear C_3 core of **2**, where the exchange Hamiltonian is[97,98]

$$H = -2J(S_1 \cdot S_2 + S_1 \cdot S_3 + S_1 \cdot S_4) - 2J'(S_2 \cdot S_3 + S_2 \cdot S_4 + S_3 \cdot S_4) \quad (5)$$

yielding the resultant energies for the tetranuclear $S_1 = S_2 = S_3 = S_4 = S_i = 2$; $S = S_1 + S_2 + S_3 + S_4$, $S' = S_2 + S_3 + S_4$ cluster,

$$E(S,S') = (J - J')[S'(S'+1)] - J[S(S+1)] + J'[3S_i(S_i+1)] + J[S_i(S_i+1)] \quad (6)$$

In the C_3 core of **2**, the O15−Mn10−O17 axis is the elongated Jahn−Teller axis for all three of the Mn10 ions. This results in misdirected magnetic orbital interactions between the Mn10 ions and concomitantly poor σ-type magnetic exchange interactions between the Mn10 ions which form the base of the tetranuclear core in **2** (Figure 9). As such, π-type exchange pathways are anticipated to dominate in the tetranuclear oxo core of **2**. Due to the long Mn10−O15 bond length, Mn10−

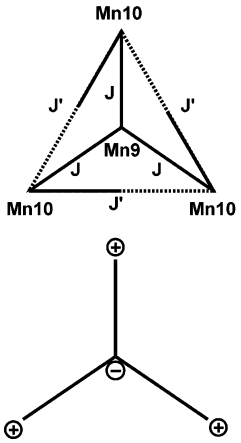

Figure 9. (Top) Antiferromagnetic exchange coupling scheme for Mn^{III}_4 core of **2**. (Bottom) Conditions describing how an $S = 4$ ground spin state can arise if $|J| \gg |J'|$. Plus and minus signs indicate orientation of the spin on each ion.

O_{oxo}−Mn10 π-type exchange is anticipated to be less than Mn10−O_{oxo}−Mn9 π-type exchange, resulting in $|J| > |J'|$. Depending on the ratio (J/J') of these antiferromagnetic exchange parameters, the ground spin state, S, for the core of **2** can be $S = 0$, 1, 2, 3, or 4. An $S = 0$ ground state results when $J \approx J'$, and the high-spin $S = 4$ state becomes the ground state when $|J| \gg |J'|$. Provided the exchange interactions between

Table 5. Comparison of Key Bond Lengths of **1** and **2**

1		2	
Mn(4)−O(5)	2.012(1)	Mn(9)−O(18)	1.988(2)
Mn(4)−O(5d)	2.012(1)	Mn(9)−O(18a)	1.988(2)
Mn(4)−O(5f)	2.012(1)	Mn(9)−O(18b)	1.988(2)
Mn(4)−O(97)	2.015(3)	Mn(9)−O(13)	2.029(2)
Mn(4)−O(97d)	2.015(3)	Mn(9)−O(13a)	2.029(2)
Mn(4)−O(97f)	2.015(3)	Mn(9)−O(13b)	2.028(2)
		Mn(10)−O(20a)	1.939(2)
		Mn(10)−O(15a)	1.957(2)
		Mn(10)−O(16a)	1.981(2)
		Mn(10)−O(13a)	2.011(2)
		Mn(10)−O(17a)	2.050(2)
		Mn(10)−O(15)	2.089(2)

the metallacryptate and the tetrahedral cores of **1** and **2** are approximately the same, this leads to an anticipated difference, ΔS, in the ground-state spin for **1** and **2** between 0 and 4. The intermediate values, $\Delta S = 2$ and 3, are in very good agreement with the difference in ground-state spin values determined by extrapolation of the $\chi'T$ data, where the ground spin state of **1** was determined to be $S = 4-5$, and that of **2** is approximately $S = 7$. As such, we anticipate that $|J| > |J'|$ for the cluster in **2**, in accord with the lower symmetry of the tetranuclear core for this cluster.

We felt it was important to identify the ultimate cause for the structural distortion of the core that leads to the altered magnetic exchange between the central four manganese ions of **1** and **2**. An examination of the structure of **2** directly provides the desired answer (Table 5). It was noted above that in **1**, the four Mn ions forming the adamantane core are equivalent, exhibiting T_d symmetry, whereas the chemically equivalent set in **2** (composed of Mn9 and Mn10) has Mn9 situated on a three-fold axis that relates the three Mn10 atoms (Figures 8 and 9). The Mn9 atom has two types of bonds at 1.99 Å (Mn9−$O_{methoxide}$) and 2.03 Å (Mn9−O_{oxide}). The other three manganese atoms (Mn10, Mn10a, and Mn10b) have six different bonds, ranging from 1.94 to 2.09 Å. The four chemically equivalent manganese atoms in **1** have all six bond lengths equivalent, at 2.01 Å. Thus, the orientation of the surface anions directly leads to this difference in core structure. In **1**, there are six equivalent azide anions bound to the metallacryptate Mn ions. Therefore, all bridging pathways from the metallacryptate manganese atoms into the central core are equivalent. In contrast, **2** contains five bound anions and a neutral solvent distributed as three hydroxide/water and three methoxide ligands. The sixth negative charge is achieved by an unbound perchlorate in the lattice. The three methoxide anions bind to Mn7 centers that are related by a three-fold axis above Mn9. The remaining hydroxides/waters are symmetrically disposed on surface Mn3 centers that interact through bridges to three Mn10 ions of the core. Thus, three of the Mn ions are related symmetrically by hydroxide/water, while a single Mn is associated with three methoxide groups.

The observed blocking temperature for **1** at 1000 Hz was determined to be 1.3 K, while the corresponding value for **2** at 1000 Hz is markedly higher, at 1.7 K, and this observation appears to be a direct result of the anion-induced structural distortions of the tetranuclear manganese core in **2**. Thus, a magnetostructural correlation emerges relating the differences in core geometry and alignment of Jahn−Teller axes with the single-molecule magnet behavior of complexes **1** and **2.** The energy barrier (E) is dependent upon two molecular factors: the ground spin state (S) and the negative axial magnetoanisotropy (D) ($E = S^2|D|$). It is likely that a higher ground-state spin for the tetranuclear manganese core in **2**, and a larger magnetoanisotropy resulting from the single ion contribution of the four Mn^{III} ions that comprise the cluster core, conspire to increase E.

Conclusions. The metallacryptate complexes **1** and **2** expand the known SMM family to include metallacrowns, a type of metallamacrocycle. These complexes are among the largest manganese clusters known to display SMM behavior and the largest with non-carboxylate ligands. In this contribution, we present a strategy to enhance both the total spin and the magnetoanisotropy of these large manganese clusters by the subtle means of anion modification. We have shown that substitution of the azide anions leads to a nearly isostructural metallacryptate that differs from the original complex by replacing the symmetrically displaced azide anions with solvent-bound anions and neutral molecules. This conversion of bound anions on the surface of the molecule is propagated to an interior adamantane core of four Mn^{III} ions. In complex **1**, all four Mn ions are structurally equivalent, whereas in **2**, one of the four manganese ions becomes chemically distinct. This distortion of the core structure leads to an orientation of Jahn−Teller axes for the remaining three core Mn^{III} ions that minimizes antiferromagnetic interactions between these three core Mn^{III} ions and maximizes the antiferromagnetic coupling to the unique atom of the core. As a consequence, the Mn_4 core in **2** is predicted to have an $S = 2$ or $S = 3$ ground state, whereas the totally symmetric core in **1** yields a diamagnetic, $S = 0$, ground state. Because these substructures are magnetically distinct, the total spin of each cluster is markedly different. We estimate that **1** has an $S = 4$ or 5 ground state, while **2** attains an $S = 7$ value. This difference in total spin, coupled with the likelihood of greater magnetoanisotropy in the less symmetric structure, leads to a significant increase in the U_{eff} values of **2** (36.2 ± 2.0 K; 25.1 ± 1.4 cm^{-1}) compared to **1** (16.5 ± 0.7 K; 11.5 ± 0.5 cm^{-1}). While there are now several examples of large metal clusters that display SMM behavior, most have lower U_{eff} values. Despite the fact that these systems often have the potential for possessing high-spin ground states, the highly symmetric structures lead to either a cancellation of individual moments or low magnetoanisotropy, or both. Our present example provides an attractive strategy to coax higher energy barriers to magnetization relaxation in large, symmetric clusters by the simple expedient of lowering the molecular symmetry by surface modification.

Acknowledgment. V.L.P. thanks the National Science Foundation (CHE-0111428) and the National Institutes of Health (GM39406) for financial support. M.L.K. acknowledges the Petroleum Research Fund (ACS PRF 38086-AC3) for financial support. This work was supported by PYTHAGORAS II to D.P.K. D.P.K. also thanks WG010 of COST action D21. C.M.Z. thanks the Horace H. Rackham Graduate School at the University of Michigan for financial support. We thank the National High Magnetic Field Laboratory (NHMFL) at Florida State University for use of their facilities, and we thank Gordon Armstrong and Alexei Souslov for their help while at the NHMFL. We also thank the Physics and Astronomy Department at Michigan State University for the use of their Quantum Design MPMS SQUID magnetometer.

Supporting Information Available: X-ray crystallographic information files of **2** (CIF). Additional figures including magnetization plots of **1** and **2**, real component of variable-temperature ac susceptibility measurements of **1** and **2**, extrapolation of $\chi'T$ data for ground spin state determination of **1** and **2**, solution state out-of-phase magnetic susceptibility of **2**, and determination of U_{eff} of **1** and **2** using the Arrhenius relationship (PDF). This material is available free of charge via the Internet at http://pubs.acs.org.

JA050951I